SEMARAK ILMU PUBLISHING

CFD Letters

Journal homepage:
https://semarakilmu.com.my/journals/index.php/CFD_Letters/index
ISSN: 2180-1363

LES Investigation of a Piston-driven Synthetic Jet Actuator with Multiple Orifices

Tung Duy Pham[1], Tomoaki Watanabe[2,*], Koji Nagata[3]

[1] Department of Aerospace Engineering, Nagoya University, Nagoya 464-8603, Japan
[2] Education and Research Center for Flight Engineering, Nagoya University, Nagoya 464-8603, Japan
[3] Department of Mechanical Engineering and Science, Kyoto University, Kyoto 615-8530, Japan

ARTICLE INFO

Article history:
Received 16 May 2023
Received in revised form 20 June 2023
Accepted 19 July 2023
Available online 5 December 2023

Keywords:
piston-driven synthetic jets; LES; compressible flows; supersonic jets

ABSTRACT

A piston-driven synthetic jet actuator has the potential for application in flow control and fundamental studies of turbulence, although the high-speed flow generated by this actuator is less investigated than a low-speed synthetic jet. The interaction of high-speed jets issued from a piston-driven synthetic jet actuator with multiple orifices is investigated with large eddy simulation (LES). The maximum jet Mach number is related to the maximum pressure inside the actuator regardless of the number of orifices. Temporal variations of the jet Mach number are almost identical for different cycles, and the jet formation in each cycle occurs under the same conditions despite the unsteady nature of the jet interaction. The phase-averaged statistics are used to examine the interaction of the synthetic jets. The converging, merging, and combined regions known for the interaction of continuous jets appear for the interaction of the high-speed synthetic jets slightly before the end of the blowing phase. However, the converging region is not clearly observed at the beginning of the blowing phase because the jets tend to be parallel to each other. Therefore, the combined region forms at a late stage of the blowing phase. Before the jets are combined, velocity fluctuations in the blowing phase become large near the furthest locations where the jets reach. Once the jets merge by their interaction, large velocity fluctuations are observed at the downstream end of the merging region. The probability density functions of velocity fluctuations in the blowing phase tend to deviate from a Gaussian distribution along the centerline of the jets. This deviation is more significant for the two-orifice model than for the four-orifice model under the same actuation frequency.

1. Introduction

Synthetic jets have been studied because of their unique property, which is formed entirely from working fluid [1]. The synthetic jet is often generated with a piezoelectric driver, which has been used to study the fundamental factors in the formation and evolution of the synthetic jet, such as the vortex pair [2]. Comparisons of synthetic jets with continuous jets are also reported in previous studies. For example, with the same Reynolds number (2000), although the mean velocity profiles between them are similar, the synthetic jets are wider in width [3]. However, the acceleration and

* *Corresponding author.*
E-mail address: watanabe.tomoaki@c.nagoya-u.jp (Tomoaki Watanabe)

https://doi.org/10.37934/cfdl.16.1.150170

deceleration of the synthetic jet affect the instantaneous velocity profile and the probability density function of the velocity time derivative, which are different from continuous jets [4]. In terms of application, synthetic jets show potential application in flow control [5]. In aerodynamics, it can delay flow separation on airfoils by reducing the thickness of the surface boundary layer. As another application in fundamental studies of turbulence, synthetic jets are often used to generate turbulence with desired properties, such as isotropic turbulence without a mean flow [6]. A random nine-synthetic-jet system can generate turbulence with large velocity fluctuations and a small mean flow [7].

The interaction of multiple continuous jets results in a complex flow field. An array of holes can be used to generate multiple jets for possible technical applications or further study. For example, four aligned jets are ejected within the boundary layer to reduce drag in film cooling [8]. Nasr *et al.,* [10] divided the jet interaction regions by converging, merging, and combining regions. The maximum of the mean streamwise velocity is reached at the combined point in the *x* direction [9]. Ghahremanian *et al.,* [10] investigated a confluent jet array and confirmed that the velocity at which the jets merge is lower than a twin jet, but the mean velocity decay is slower. For the jet interaction, there are also linear relationships between the nozzle spacing extension and the streamwise location of the combining/merging points [11], and between the separation length and the merging point location [12]. The jet spacing also has a significant influence on the production of vortices [13]. Theoretical power laws for kinetic energy spectra of turbulence are often observed in a single turbulent jet [14]. It is also evaluated in the interaction regions of multiple jets [15]. The interaction results in the non-Kolmogorov -5/3 spectrum of streamwise velocity fluctuations [16]. In addition, the relationship between extreme events and the -5/3 law is proved for the jet interaction [17].

Regarding the interaction of multiple synthetic jets, Smith *et al.,* [18] showed that the phase angle affects the path of the newly merged vortex pair due to the strong entrainment of ambient fluid. In contrast, the direction of the merged jets depends on the initial phase with a significant relative phase of the two jets [19]. With a modified design, the incline synthetic jet array can attain a peak velocity of up to 100 m/s [20]. Jankee *et al.,* [21] showed that the multiple synthetic jets are efficient in separation control and drag reduction when the orifice spacing is smaller than 6.5 times the orifice diameter. Another application of synthetic jet array is utilized for the enhancement of heat transfer in the heat sinks for electronics cooling. Cavity size, shape and orifice length are parameters that affect heat transfer performance [22]. In addition, at a high vibration amplitude, the large opening angle of the orifice largely affects the performance [23]. Coupling with the cross-flow of 14.7 m/s and 8 m/s, the activation of the synthetic jet array contributes up to 9.3 % and 23.1 % of the heat transfer coefficient, respectively [24].

However, with conventional synthetic jets, there are some limitations related to the frequency of oscillations, the material for the diaphragm, and even the power input. These limitations have been significantly overcome through the development of piston synthetic jet actuators (PSJAs), which can provide a high-speed regime [25]. It can achieve full-scale application when the peak velocity reaches 124 m/s [26]. By using PSJA, the highest lift coefficient ascends by 80%, and the stall angle changes from 12 to 18 deg. [27]. In one of the latest experiments with PSJ in the case of the single orifice, the flow velocity can reach approximately Mach 1.6 [28]. Crittenden *et al.,* [25] studied the parameters affecting the velocity characteristics, including actuation frequency, piston stroke length, and compression ratio. The compressibility effect relates to the pressure asymmetry during the blowing and suction phases. In addition, there is a correlation between the maximum Mach number and the maximum pressure inside the actuator [28]. This correlation is also found in a numerical model [29]. The PSJs are also used to generate compressible turbulence by the interaction of supersonic synthetic jets. The compressible turbulence chamber was developed with the opposition of the jet arrays,

which generates nearly homogeneous and isotropic turbulence with a small mean velocity at the chamber center [30]. Furthermore, the compressible homogeneous and isotropic turbulence generated by the PSJAs was investigated to evaluate compressibility effects on the statistical properties of turbulence [31].

Although high-speed synthetic jets generated from multiple orifices of PSJs have potential applications for flow control and fundamental studies of turbulence, such flows have hardly been investigated. Sakakibara *et al.,* [28] characterized the performance of the PSJA with two or four orifices with the pressure measurement inside the actuator and flow visualization. However, the flow field formed by the interaction of the multiple synthetic jets has not been investigated in detail. The present study reports numerical simulations of a multi-orifice PSJA. The performance of the simulated PSJA is tested by comparing the pressure variation in the actuator and the pressure dependence of the maximum jet Mach number with experimental data. In addition, the interaction of multiple synthetic jets is investigated with velocity statistics. The details of the numerical simulations are presented in Sec. 2, while the results are discussed in Sec. 3. The paper is summarized in Sec. 4.

2. Numerical Procedures

2.1 Numerical Model of Piston Synthetic Jet Actuators

A numerical model of the PSJA is based on the experimental study by Sakakibara *et al.,* [28]. The PSJA consists of a piston/cylinder actuator with an orifice plate at the top of the cylinder. In experiments, the actuator part is often developed based on a model engine, and the piston is driven with a motor. We consider the PSJAs with two or four orifices, as shown in Figure 1. The basic dimensions also follow the experiment [28]. Here, we use square orifices instead of the round orifice to simplify the computational model, although synthetic jets often use the latter. Our previous study has confirmed that the performance of the PSJA is similar for square and round orifices as long as the orifice area is identical [29]. For both two- and four-orifices models, the side dimension of square orifices is d = 2 mm. They are placed in symmetrical positions at a distance of 2 mm and in the center of the top wall of a square cylinder with a sidelength of 24 mm. The length of the cylinder is L_x = 21.7 mm, which also determines the bottom dead center (BDC) position for the piston. With a piston stroke of L = 20.6 mm, the top dead center (TDC) position will be 1.1 mm from the top of the cylinder. Here, the piston movement is described by the cosine function with a frequency f, and the details will be described in the following section. A point marked as P is the point for sampling pressure and temperature in the cylinder. The location of this point is determined in the same way as in the experiment when a pressure transducer is installed [28]. Its position is centered on the segment from the edge of the square orifice to the edge of the cylinder.

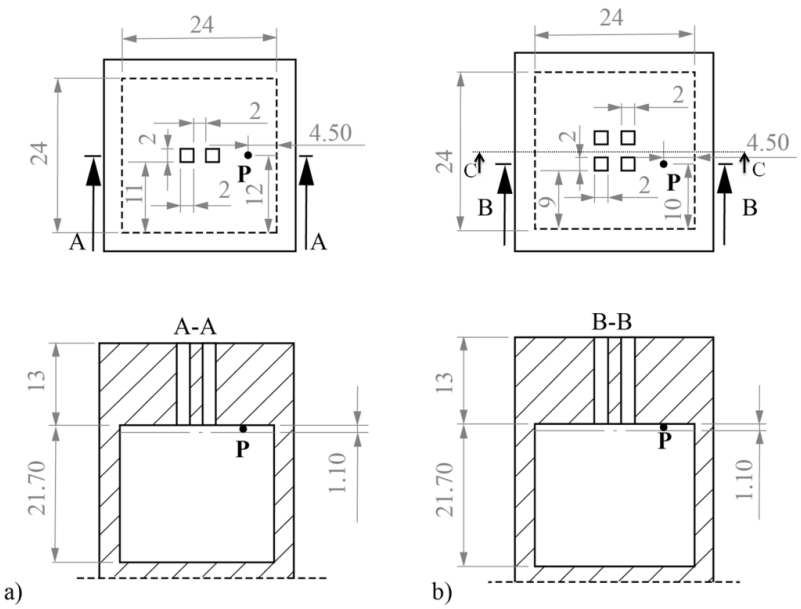

Fig. 1. Piston synthetic jet actuators (PSJAs): a) two-orifice model; b) four-orifice model (all dimensions are in mm)

2.2 Computational Domain and Numerical Methodology

The computational domain consists of three parts: the piston/cylinder part for piston movement, the outflow part where the synthetic jet forms, and the orifice part which connects the other two parts, as shown in Figure 2a. The orifice parts have two orifices or four orifices depending on the models. The rectangular blocks are used for these parts. With the two-orifice model, each part has a size of (*Lx, Ly, Lz*) listed in Table 1. The coordinate origin of this model is set at the center of two orifices. Similarly, with the four-orifice model, each part has its parameters listed in Table 2. Its coordinate origin is set at the center of the four orifices outlet.

Large eddy simulation (LES) is performed with OpenFOAM. The numerical method is the same as in our previous study of a PSJA with a single orifice [29], where the LES results are compared with experiments. LES is used for accurate simulations of the unsteady formation of the synthetic jets. The *blockMesh* utility of OpenFOAM is used for meshing. The smallest mesh size at the domain center is 0.5 mm, and the cell-to-cell ratio is 1.05. Figure 2b shows a slice through the center of two orifices, and a part of the region of interest is shown in Figure 2c.

The governing equations are compressible Navier—Stokes equations. The LES solves the low-pass-filtered conservation equations of mass, momentum, and energy, which are expressed as follows [32]:

$$\frac{\partial \bar{\rho}}{\partial t} + \frac{\partial \bar{\rho}\tilde{u}_j}{\partial x_j} = 0, \tag{1}$$

$$\frac{\partial \bar{\rho}\tilde{u}_i}{\partial t} + \frac{\partial \bar{\rho}\tilde{u}_i\tilde{u}_j}{\partial x_j} = -\frac{\partial \bar{p}}{\partial x_i} + \frac{\partial}{\partial x_j}\left(\bar{\tau}_{ij} - \tau_{ij}^{sgs}\right), \tag{2}$$

$$\frac{\partial \bar{\rho}\tilde{E}}{\partial t} + \frac{\partial}{\partial x_j}\left[\left(\bar{\rho}\,\tilde{E} + p\right)\tilde{u}_j\right] = \frac{\partial}{\partial x_j}\left(\lambda\frac{\partial \tilde{T}}{\partial x_j} + \tilde{u}_j\bar{\tau}_{ij} - H^{sgs} - \sigma^{sgs}\right), \tag{3}$$

With the equation of state for the ideal gas $\bar{p} = \bar{\rho}R\tilde{T}$. Here, $\bar{*}$ and $\tilde{*}$ are filtered and density-weighted filtered variables, respectively. $\bar{\rho}$ and $\bar{p}$ are the filtered density and pressure, respectively,

$\tilde{u}_j$ (j = 1, 2, 3) is the filtered velocity vector, $\bar{\tau}_{ij}$ is the filtered viscous stress tensor. $\tilde{E}$ is the filtered total energy, $\tilde{T}$ is the filtered temperature. λ is the molecular thermal diffusivity. H^{sgs} is the sub-grid enthalpy flux and σ^{sgs} is the sub-grid viscous work.

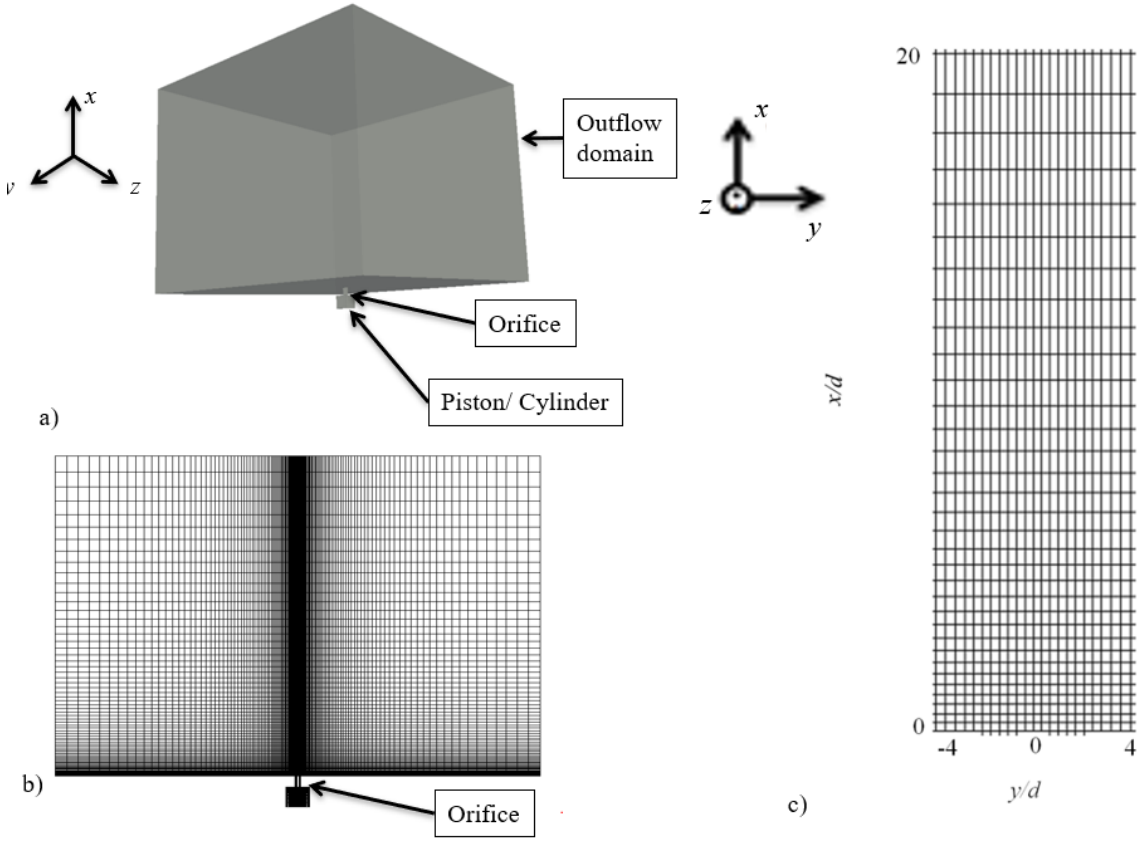

Fig. 2. a) The computational domain; b) the grid distribution on the center plane *xy* through two orifices; c) the grid distribution of the orifice area

Table 1
The domain sizes and the numbers of cells for the two-orifice model

Domain	Size (mm) (*Lx, Ly, Lz*)	Number of cells (*Nx, Ny, Nz*)
Piston/Cylinder	(21.7, 24, 24)	(24, 38, 34)
Orifice	(13, 2, 2) ×2	(26, 4, 4) ×2
Outflow domain	(360, 486, 482)	(74, 144, 136)

Table 2
The domain sizes and the numbers of cells for the four-orifice model

Domain	Size (mm) (*Lx, Ly, Lz*)	Number of cells (*Nx, Ny, Nz*)
Piston/Cylinder	(21.7, 24, 24)	(24, 38, 38)
Orifice	(13, 2, 2) ×4	(26, 4, 4) ×4
Outflow domain	(360, 486, 486)	(74, 144, 144)

The bottom wall of the computational domain in the cylinder part is set as the top surface of the piston. The piston movement is modeled by the movement of the computational boundary at the bottom. By this setting, the cell size of the cylinder part is varied by time *t*. The piston periodically

moves between the BDC and TDC in Figure 3a with the velocity U_p shown in Figure 3b. For a sinusoidal time history of the piston velocity, the piston position x_P is given by a cosine function as

$$x_p = x_c + \frac{1}{2} L cos(2\pi f t + \omega_0), \tag{4}$$

where the center location of the piston movement is $x_c = -24.4$ mm and $\omega_0 = \pi$ is the initial phase. Time t is normalized by a period of one cycle $T = 1/f$, where the frequency f is given as a computational parameter.

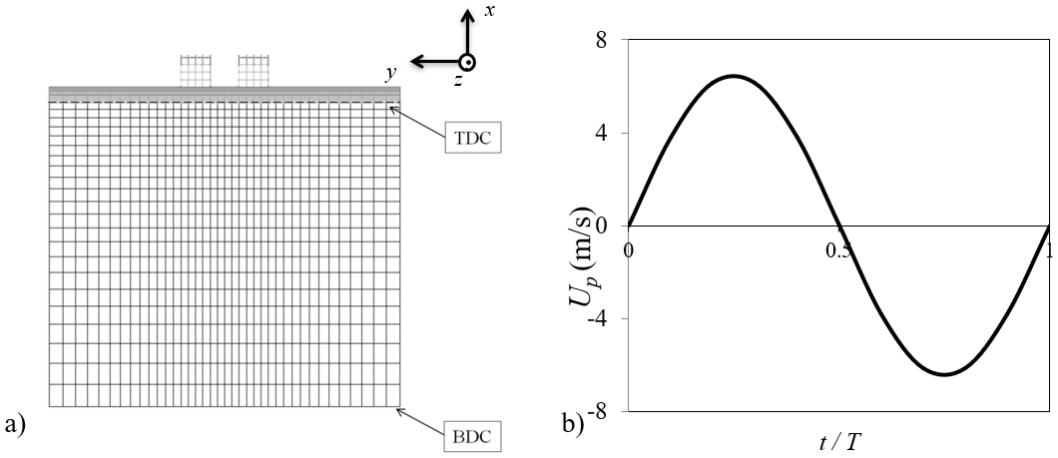

Fig. 3. a) The grid distribution for the piston located at the TDC or BDC b) Piston velocity

The numerical method, boundary conditions, and initial conditions are the same as the simulation of one orifice model [29]. An ideal gas (air) is the working fluid. LES with the Smagorinsky model using rhoPimpleFoam is applied. The *waveTransmissive* boundary condition, which is a non-reflecting boundary condition, is applied for the outflow domain. Due to the movement of the piston, its boundary condition is applied by *movingWallVelocity* at the bottom of the computational domain, which corresponds to the top surface of the piston. For both models, simulations are conducted for f = 50, 75, 100, 125, and 150 Hz. Flow statistics are evaluated with phase averages, which are taken with time series data over 20*T.* The initial pressure and temperature T_0 are the atmospheric pressure P_{atm} = 101,325 Pa and 300 K, respectively.

3. Results

3.1 Pressure Histories inside the Cylinder

The pressure inside the cylinder is a characteristic parameter related to the jet velocity [28]. The pressure taken at point P inside the cylinder (Figure 1) is compared with the measurement results of experiments. The verification with the single orifice for different frequencies shows a good agreement between the simulation and experimental result [29]. For the two-orifice case at 100 Hz, we compare these pressure histories in Figure 4, which presents the absolute pressure P normalized by P_{atm}, $P_r = P/P_{atm}$. Here, t/T = 0 and 1 indicate that the piston is at the BDC while t_{peak} is the time at which the maximum pressure is achieved. The simulation (Sim.) and experiment by Sakakibara *et al.,* [28] agree well in terms of both peak and temporal variation. When comparing with experiments by Eri *et al.,* [33], with the same frequency of 100 Hz, the difference is observed for the maximum

pressure because of the differences in the volume displacement and the areas of the orifice exit. However, the overall shape of the pressure history is similar. Both numerical and experimental results exhibit a highly non-symmetric pressure variation, which is a signature of a high-speed synthetic jet. This comparison further validates the present numerical model of the PSJA.

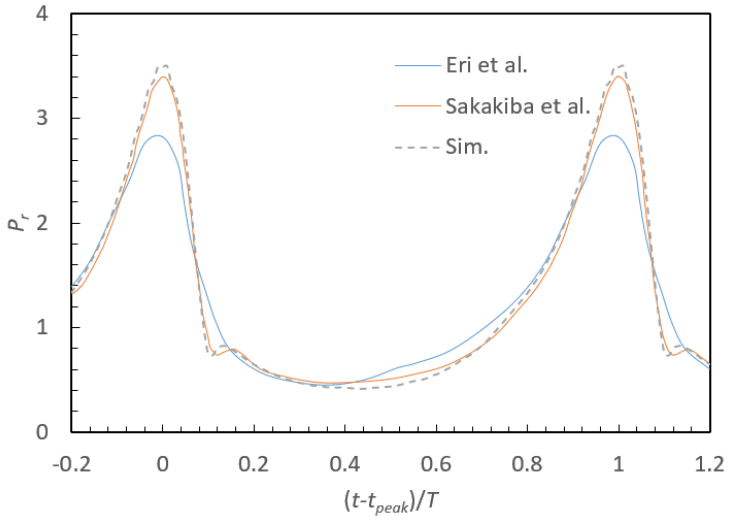

Fig. 4. Comparison of normalized pressure between the simulation (Sim.) and experiments with the two-orifice case at 100 Hz

Figures 5 and 6 show time histories of P_r over two cycles for f = 50, 75, 100, and 150 Hz for the two- and four-orifice models. There is only a minimal difference in the pressure variations for the two different cycles, indicating that similar synthetic jets form in each cycle. In addition, the pressure variations are highly asymmetric despite the piston movement described by the cosine function. As the frequency increases, the maximum pressure becomes larger, and the minimum pressure becomes smaller. This is consistent with the experimental results from Sakakibara *et al.,* [28] for both two- and four-orifice cases.

LES for different frequencies indicates that a peak pressure can be attained later in terms of time (t_{peak}/T) for a higher frequency. For the two-orifice model, the values of t_{peak}/T are 0.365, 0.399, 0.420, and 0.439 for f = 50, 75, 100, and 150 Hz, respectively. For the four-orifice model, the values of t_{peak}/T are 0.275, 0.305, 0.360, and 0.394 for f = 50, 75, 100, and 150 Hz, respectively. As f increases, they shift to the middle of the cycle. The trend is the same in the case of a single orifice [29]. In addition, by comparing the maximum pressure at a given frequency in Figures 5 and 6, the maximum pressure in one cycle is more considerable when the total orifice area is smaller [28].

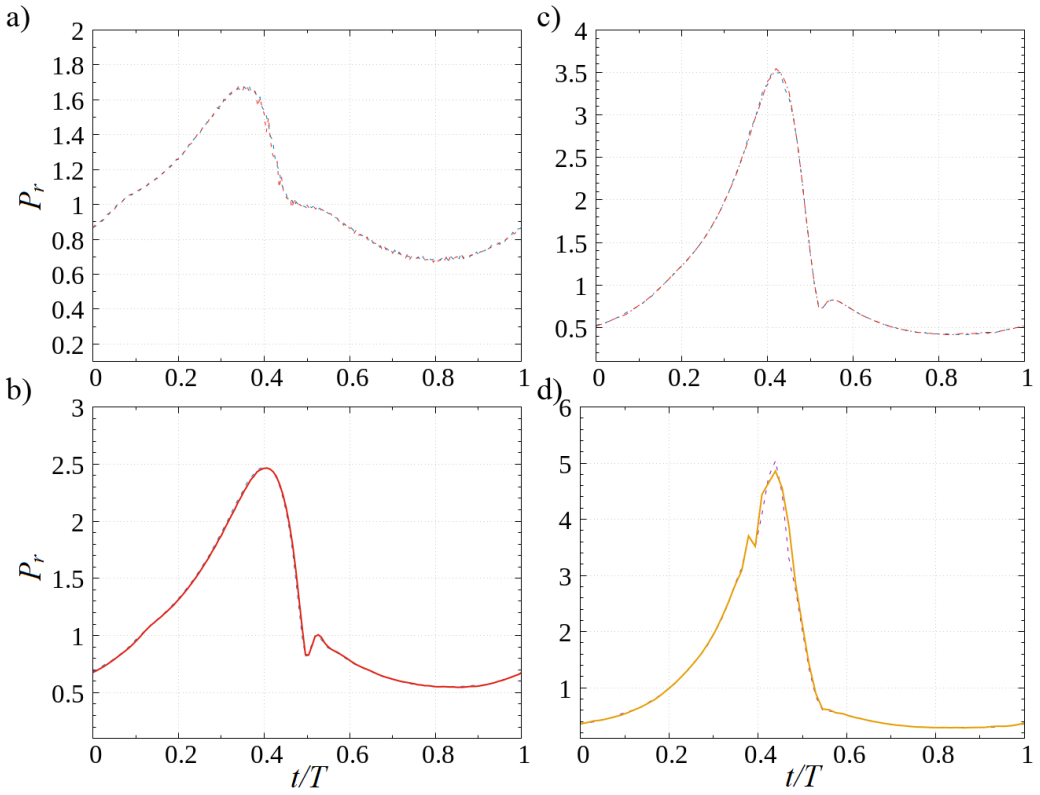

Fig. 5. Comparison of normalized pressure P_r for $0 \leq t/T \leq 1$ between two different cycles for the two-orifice model: a) f = 50 Hz; b) f = 75 Hz; c) f = 100 Hz; d) f = 150 Hz

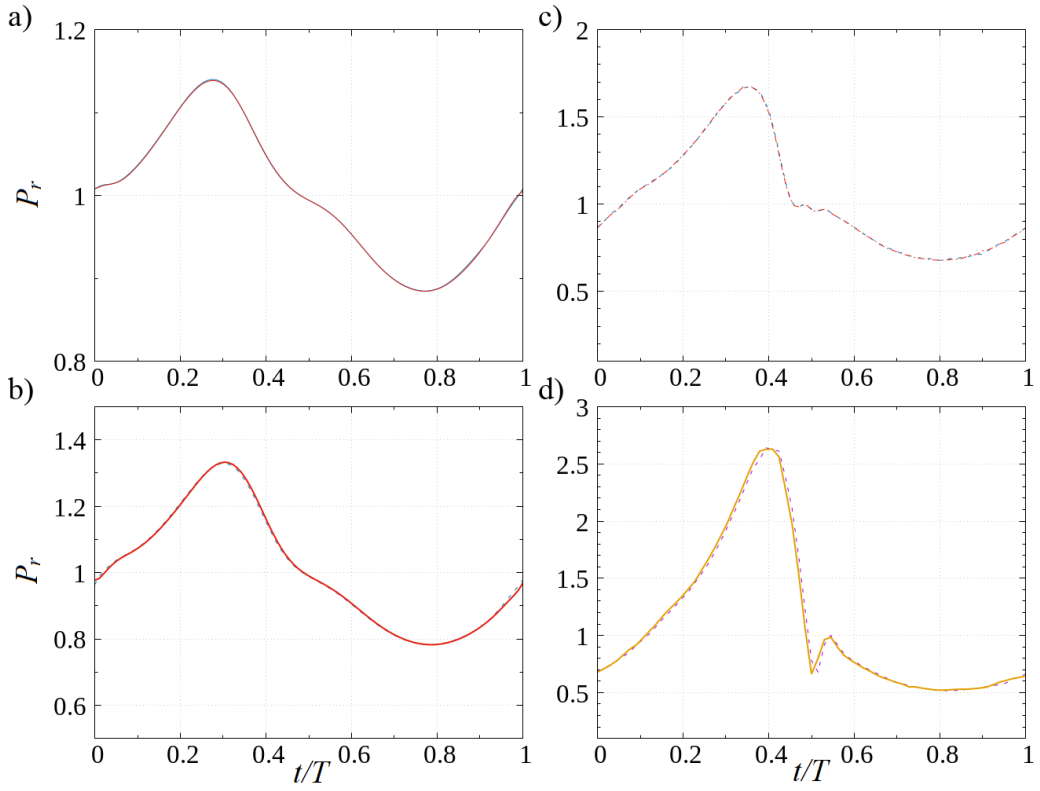

Fig. 6. Comparison of normalized pressure P_r for $0 \leq t/T \leq 1$ between two different cycles for the four-orifice model: a) f = 50 Hz; b) f = 75 Hz; c) f = 100 Hz; d) f = 150 Hz

3.2 Jet Mach Number History

The jet Mach number $M = |u|/a$ is evaluated with a fluid velocity u and the speed of sound a at the exit of one of the orifices. Figures 7 and 8 show the time history of M for two- and four-orifice models. Here, the results for two cycles are shown for comparison. The variation of the Mach number hardly depends on the cycles, and the jet Mach number depends solely on the phases for each case. In the blowing phase, the Mach number increases with time and reaches the largest value. Then, it decreases with time until the end of the blowing phase. Finally, M slightly increases in the suction phase. The plots of M show that the middle of the cycle at $t/T = 0.5$ is the transition time between the blowing and suction phases. There are small effects of velocities in y-and z-directions so M is not exactly zero at $t/T = 0.5$ at higher frequencies. The maximum Mach number is achieved at $t/T = 0.375$, 0.406, 0.430, and 0.455, respectively, for $f = 50$, 75, 100, and 150 Hz for the two-orifice model. These times are respectively $t/T = 0.305$, 0.323, 0.360, and 0.410 for the four-orifice case. They are close to the times at which the pressure reaches the maximum.

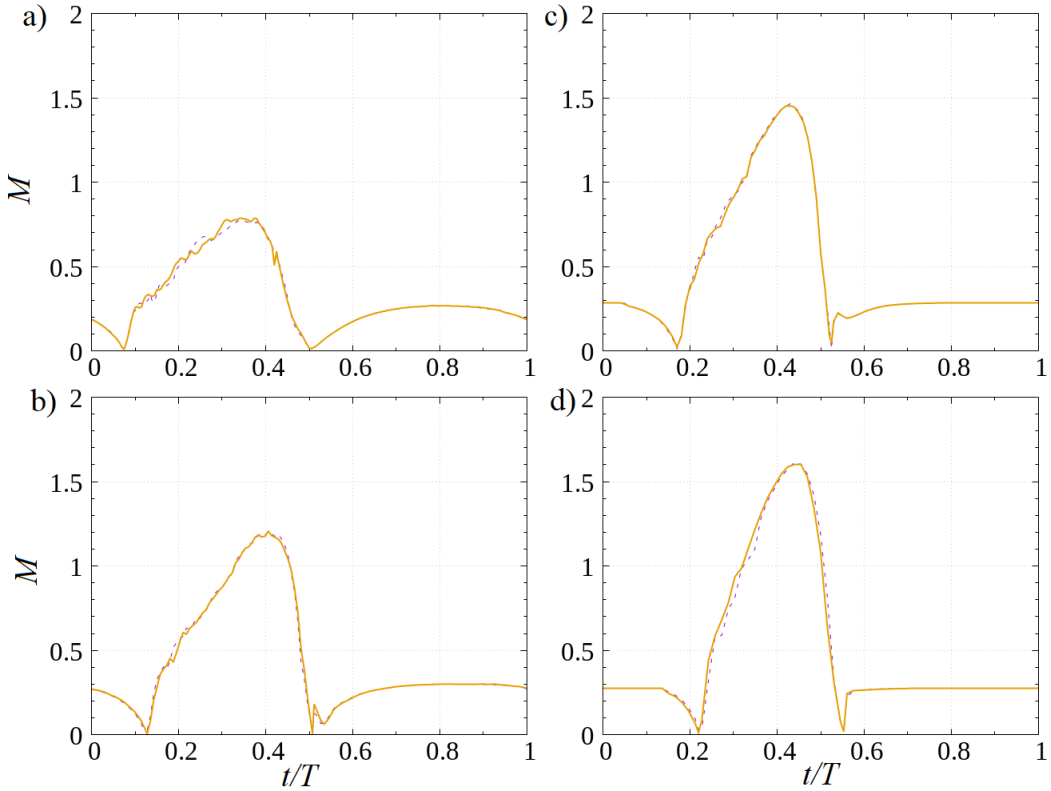

Fig. 7. Mach number histories at the orifice exit for the two-orifice model: a) $f = 50$ Hz; b) $f = 75$ Hz; c) $f = 100$ Hz; d) $f = 150$ Hz

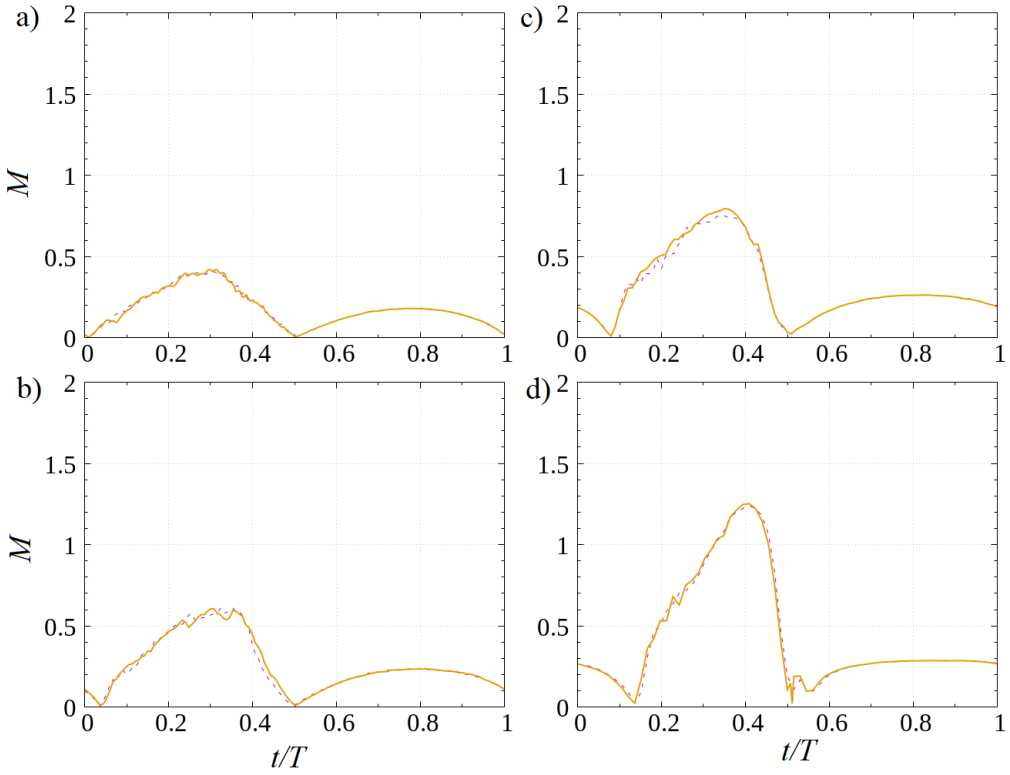

Fig. 8. Mach number histories at the orifice exit for different frequencies for the four-orifice model: a) f = 50 Hz; b) f = 75 Hz; c) f = 100 Hz; d) f = 150 Hz

For a single-orifice case, the following relation has been confirmed for the maximum Mach number M_{max} and the maximum pressure P_{rmax} [34]

$$M_{max} = \left\{ \frac{2}{\gamma - 1} \left(P_{rmax}^{\frac{\gamma-1}{\gamma}} - 1 \right) \right\}^{1/2}, \tag{5}$$

with the specific heat ratio γ being 1.4 [7, 26]. Figure 9 compares the present LES results of M_{max} and P_{rmax} with Eq. (5). Case A represents the two-orifice model, and case B represents the four-orifice model. Eq. (5) well describes the relation between M_{max} and P_{rmax} for multiple-orifice cases and is useful for estimating the jet Mach number with the pressure measurement.

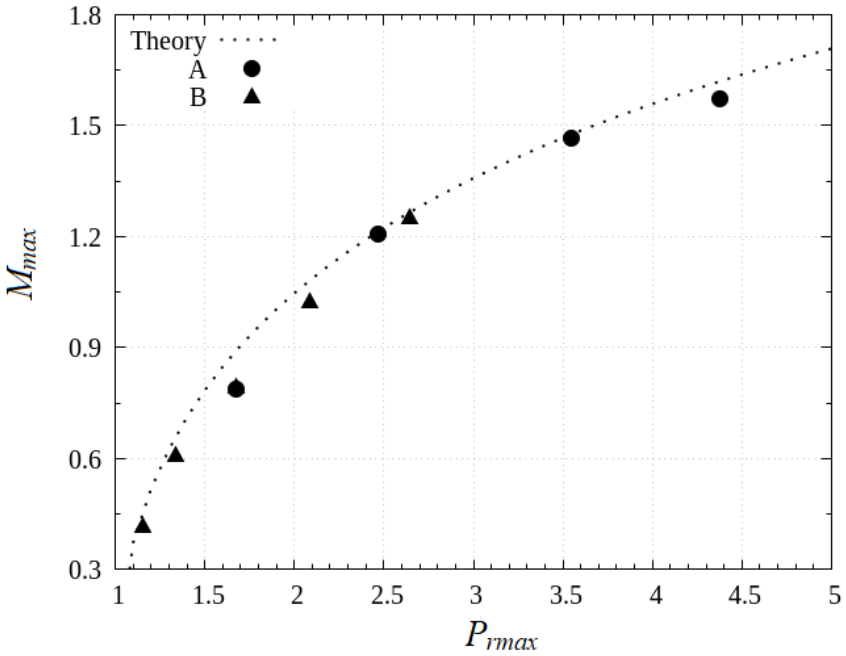

Fig. 9. Relationship between the maximum pressure and the maximum jet Mach number for the two-orifice model (A) and the four-orifice model (B)

3.3 Phase-averaged Flow-field

In this section, we will discuss the mean velocity and root-mean-square (rms) velocity fluctuations defined with phase averages. The averages are evaluated as functions of time in the phase from t = 0 to T. The phase-averaged velocity in the x direction is denoted by U, while the rms value of velocity fluctuations, u_{rms}, are evaluated as the root-mean-square of velocity fluctuations from U.

3.3.1 Two-orifice case

Figure 10 presents the phase-averaged velocity in the x direction on the plane that crosses the center of the orifices for f = 100 Hz. To evaluate the interaction between these two parallel jets, the phase-averaged velocity at the center line between these two jets is also shown in Figure 11. Here, y = 0 is the midpoint between the two orifices. The blowing and suction phases correspond to t/T = 0.1—0.5 and 0.5—1, respectively. In Figure 10, we can observe the growth of the jets in the blowing phase. The two jets tend to interact to form a converging region, then create a merging region where they meet each other, and become a single jet in a combined region. A similar transition was also found for two continuous parallel jets [9]. The converging region is observed near the orifice when the velocity of the jets is high, e.g., $x/d \lesssim 5$ at t/T = 0.4, where the mean velocity increases with x along the centerline in Figure 11d. The flow induced by a PSJA with two round orifices was visualized with a shadowgraph technique [28]. They also observed that the converging region forms for $x/d \lesssim 5$ for the case of two-orifice jets at 100 Hz. For the present LES, the merging region is approximately in the range of $5 < x/d < 35$. At an early time in the cycle, when the jets are being formed in Figures 10b-c, the two jets align with the x direction and spread in the vertical direction resulting in the interaction of the jets. At a later time, the jets are inclined to the other jet in Figure 10e, resulting in the formation of the merging and combined regions. Because the inclination of the jets occurs at a late time of the blowing phase, the merging and combined regions move with time. In Figure 9e, the

jets merge at about x/d = 25. The inclination of the jets causes the converging and merging regions to be closer to the orifices. In Figure 10e, the converging region already appears at about x/d = 2. Figure 11 indicates that the mean velocity along the centerline between the orifices reaches 250 m/s at the maximum. The formation of the merging and combining regions is also confirmed by the increase of the mean velocity with x in Figures 11b-e. In Figure 11a, a negative mean velocity is observed near the wall, which is related to the flows into the orifices from outside. Thus, the induced flow in the suction phase still affects the flow at the moment when the piston is going upward. In the suction phase after t/T = 0.5, the flow toward the top wall of the PSJA is observed as a negative mean velocity. However, this velocity is not as large as the mean velocity in the blowing phase.

Figure 12 plots u_{rms} on the same centerline as in Figure 11. In Figures 11b-e, the merging and combined regions have a large mean velocity during the blowing phase. The regions with large u_{rms} in Figures 12b-e approximately agree with those with a large mean velocity of the merging and combined regions, and the interaction between the two synthetic jets causes large velocity fluctuations. The maximum value of the rms velocity fluctuations reaches 80 m/s, which is expected to be large enough for fluid compression and expansion due to turbulent motions affecting the flow. As also found for the mean velocity, u_{rms} in the suction phase is very small.

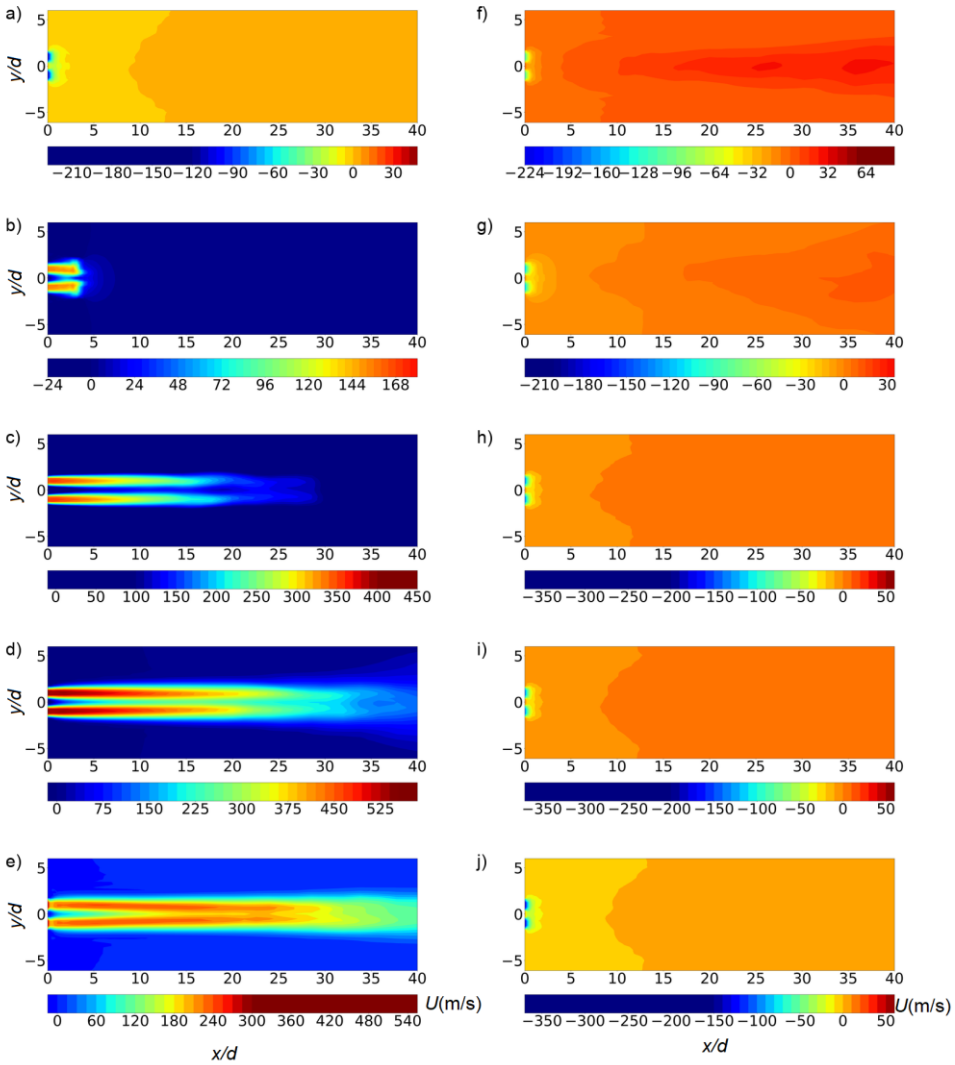

Fig. 10. Phase-averaged velocity in the x-direction for f = 100 Hz at a) t/T = 0.1, b) 0.2, c) 0.3, d) 0.4, e) 0.5, f) 0.6, g) 0.7, h) 0.8, i) 0.9, and j) 1.0, for the two-orifice model

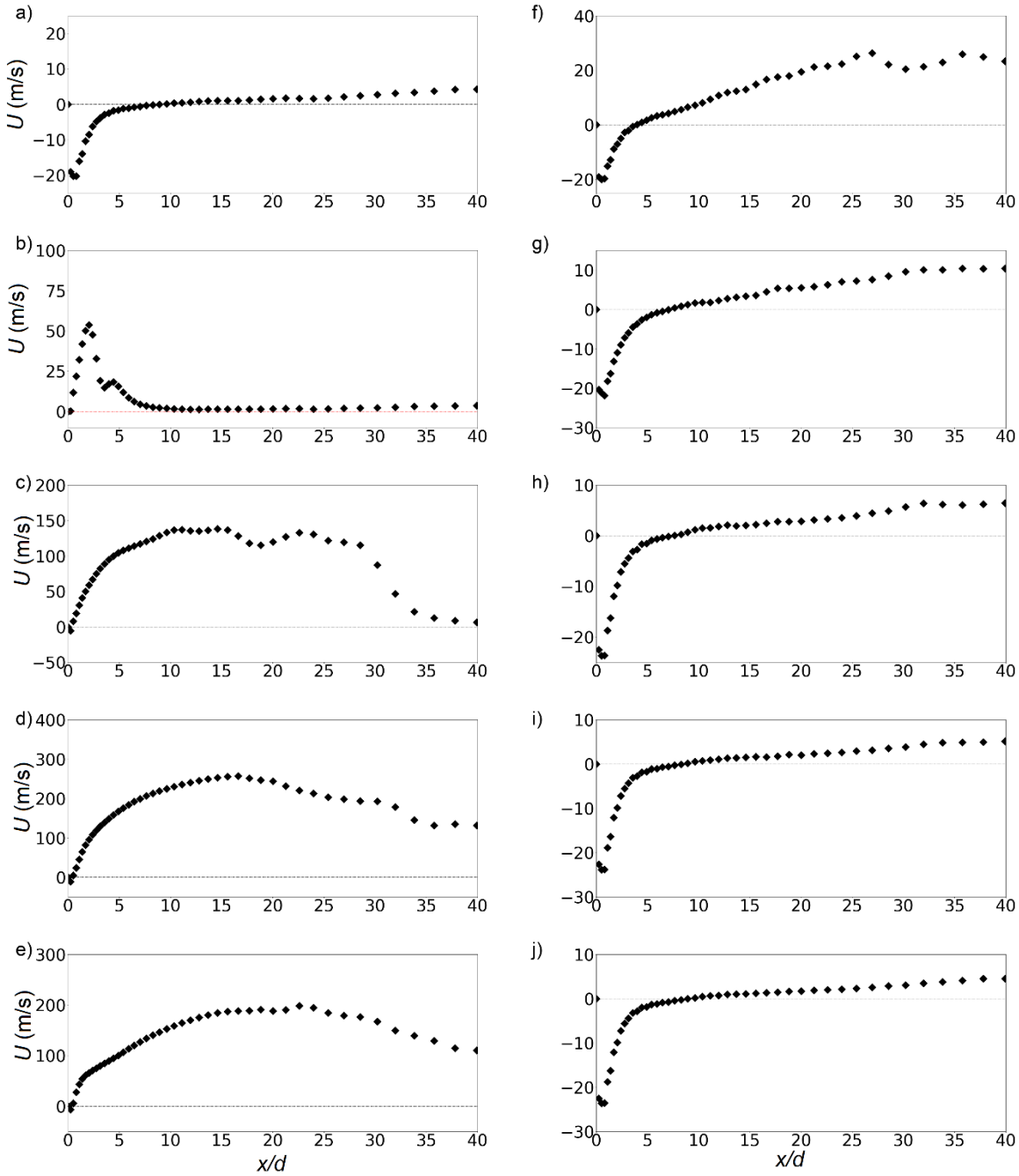

Fig. 11. Phase-averaged velocity in the *x* direction along the centerline for *f* = 100 Hz, at a) *t/T* = 0.1, b) 0.2, c) 0.3, d) 0.4, e) 0.5, f) 0.6, g) 0.7, h) 0.8, i) 0.9, and j) 1.0, for the two-orifice model

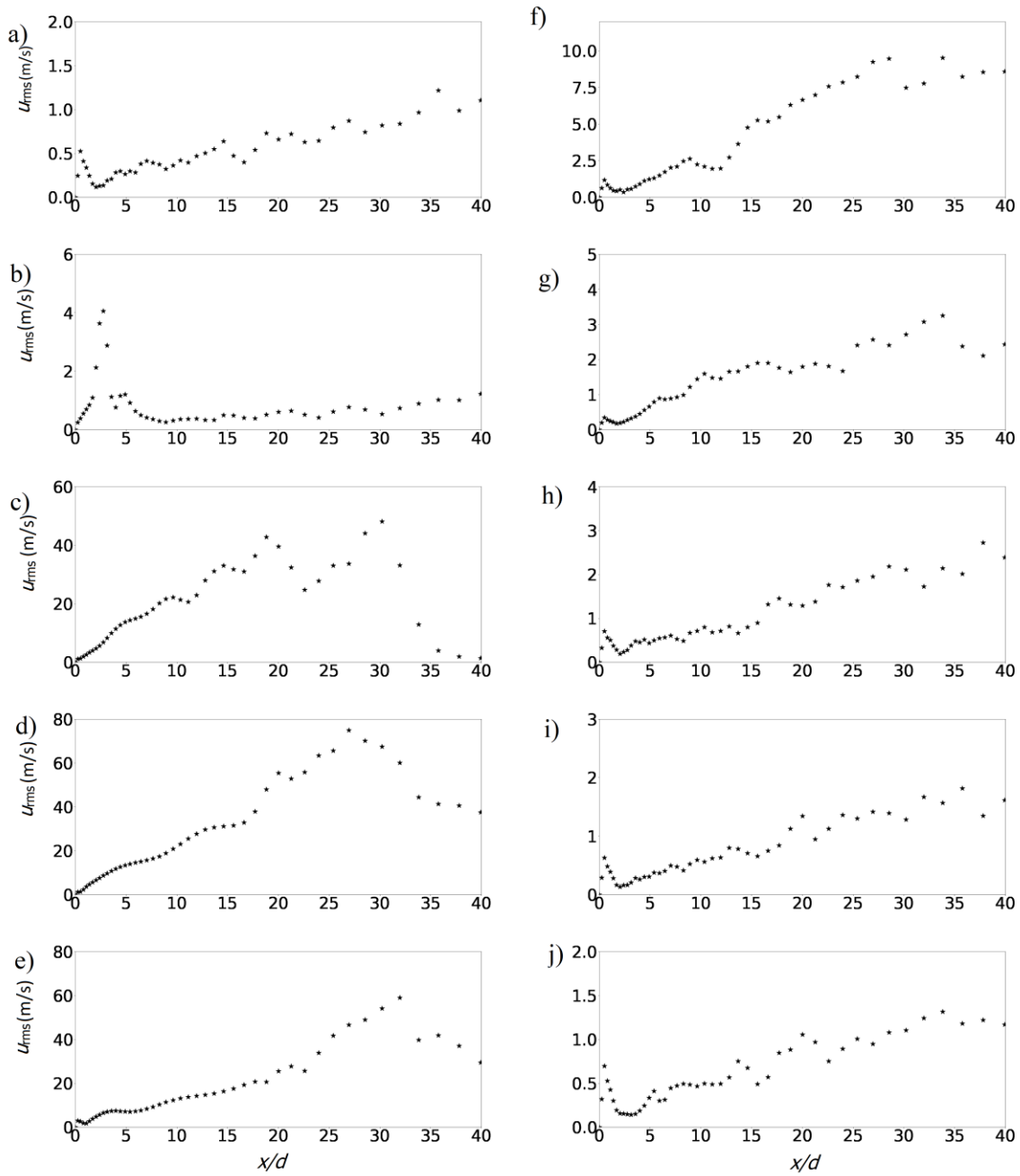

Fig. 12. Distributions of rms fluctuations of velocity in the *x* direction, u_{rms}, along the centreline of the A-A plane in Figure 1b of the two-orifice model with *f* = 100 Hz: a) *t/T* = 0.1, b) 0.2, c) 0.3, d) 0.4, e) 0.5, f) 0.6, g) 0.7, h) 0.8, i) 0.9, and j) 1.0

3.3.2 Four-orifice case

For the case of four orifices, the mean velocity and rms velocity fluctuations are presented at the center of four orifices, i.e., the C-C plane in Figure 1b. The results for the four-orifice model are also presented for *f* = 100 Hz. For this case, the maximum Mach number is about 1, which is smaller than that for the two orifices with the same frequency because of the difference in the total orifice area.

Figure 13 shows the phase-averaged velocity from *t*/*T* = 0.1 to 1.0 for the four-orifice model. Because the C-C plane does not pass through any orifice, the velocity also asymptotes to 0 toward *x* = 0, which is the top surface of the PSJA. The interaction of the four jets induces the mean velocity

on this plane in the blowing phase (Figures 13b-e). At the end of the blowing phase in Figure 13e, the four jets are fully combined forming a single jet with a large mean velocity along the centerline. The jets have not fully merged yet at an early time in Figures 13b-d, where the large mean velocity in each jet can be identified. This time-dependent behavior of the jet interaction is generally in good agreement with the two orifices model.

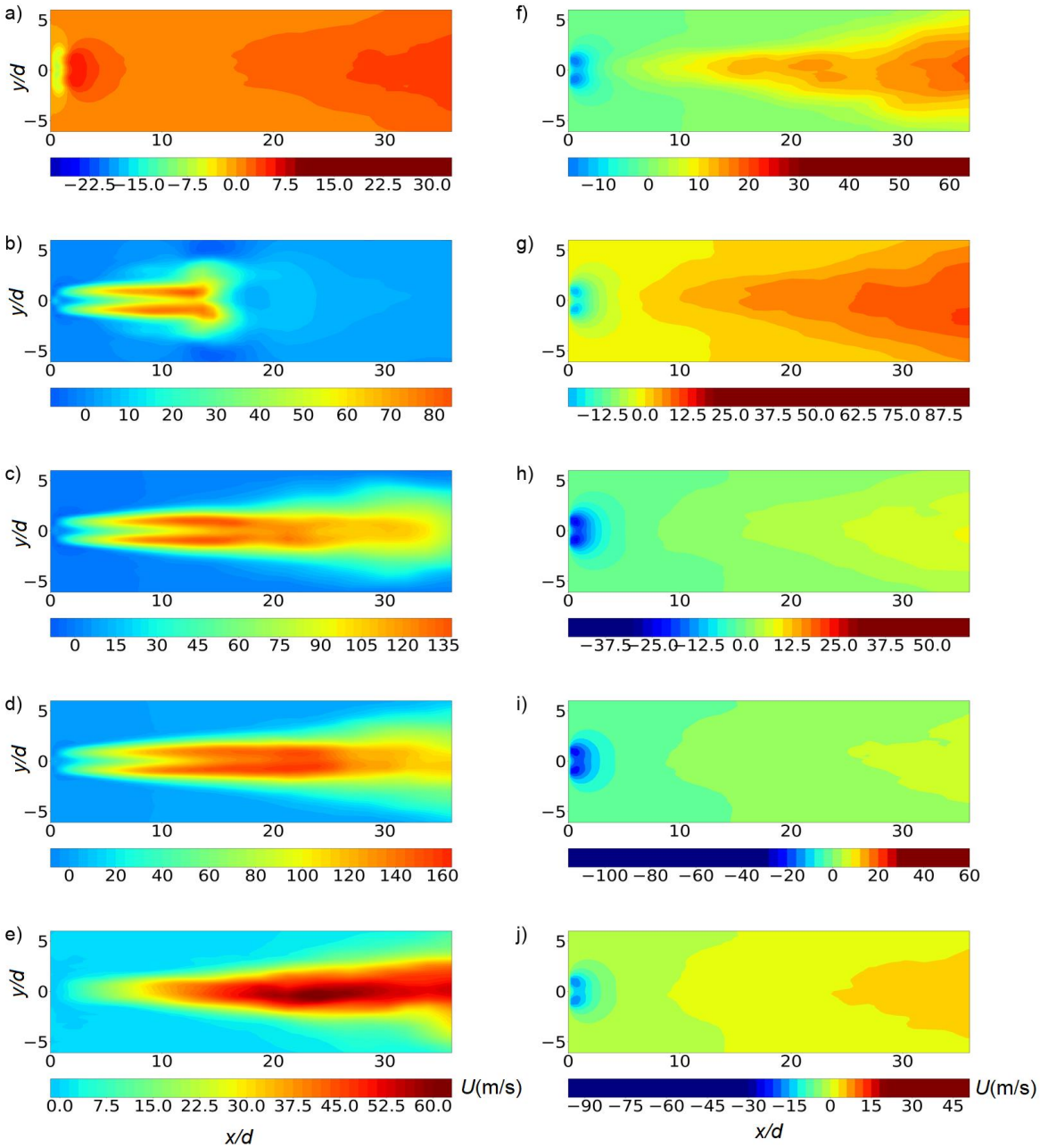

Fig. 13. Phase-averaged velocity in the *x* direction for *f* = 100 Hz at a) t/T = 0.1, b) 0.2, c) 0.3, d) 0.4, e) 0.5, f) 0.6, g) 0.7, h) 0.8, i) 0.9, and j) 1.0, at C-C plane in Figure 1b for the four-orifice model

Figure 14 shows the rms velocity fluctuations along the centerline of the four orifices. At *t/T* = 0.2, the mean velocity decreases at about *x/d* = 14 in Figure 13b. The rms fluctuations also become small beyond this location. Therefore, the velocity fluctuations are large at the streamwise end of the jets. For *t/T* = 0.3-0.5, the rms fluctuations tend to increase with *x*. This will be explained in the next

section with the instantaneous velocity profile. In the suction phase, as *x*/d increases, rms fluctuations also tend to grow, as expected from the remnant of the jets generated in the blowing phase.

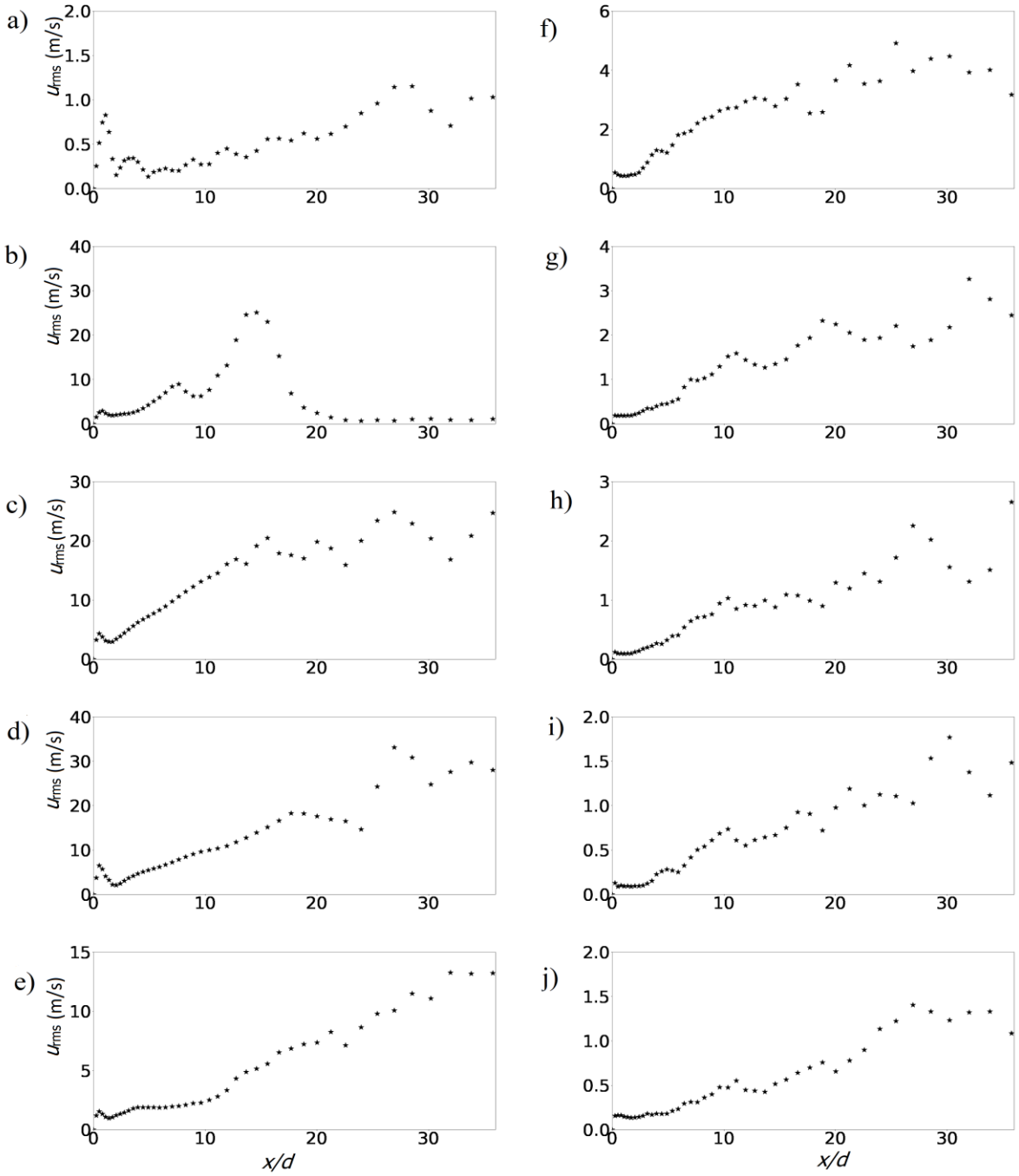

Fig. 14. Distributions of rms fluctuations of velocity in the *x* direction, u_{rms}, along the centreline (*y* = 0) of the C-C plane in Figure 1b of the four-orifice model with *f* = 100 Hz: a) *t*/*T* = 0.1, b) 0.2, c) 0.3, d) 0.4, e) 0.5, f) 0.6, g) 0.7, h) 0.8, i) 0.9, and j) 1.0

Figure 15 shows the time-averaged streamwise velocity along the centerline of the two-orifice case (*f* = 100 Hz). The mean velocity along the centerline is negative near the orifice (about *x*/*d* < 1), rapidly increases with *x* up to about *x*/*d* = 5, and varies slowly with *x* for the further downstream region. One of the important parameters for the synthetic jet interaction is the ratio *R* between the

orifice spacing and side length of the orifice, which is 2 for the present two-orifice model. The interaction of two low-speed synthetic jets was investigated by Kim *et al.,* [35], where one of the experiments also considered R = 2. The present result is similar to their experimental results. They also observed a negative mean streamwise velocity along the centerline near the orifice (about x/d < 1.4) and a rapid increase with x up to about x/d = 6. The distribution of the mean velocity strongly depends on turbulence, as the Reynolds stresses due to velocity fluctuations significantly contribute to the momentum flux, which is dominated by large-scale velocity fluctuations. The agreement with the experiments [35] suggests that the large-scale turbulent motions are accurately simulated in the present LES and that the jet interaction is similar for both high-speed and low-speed synthetic jets.

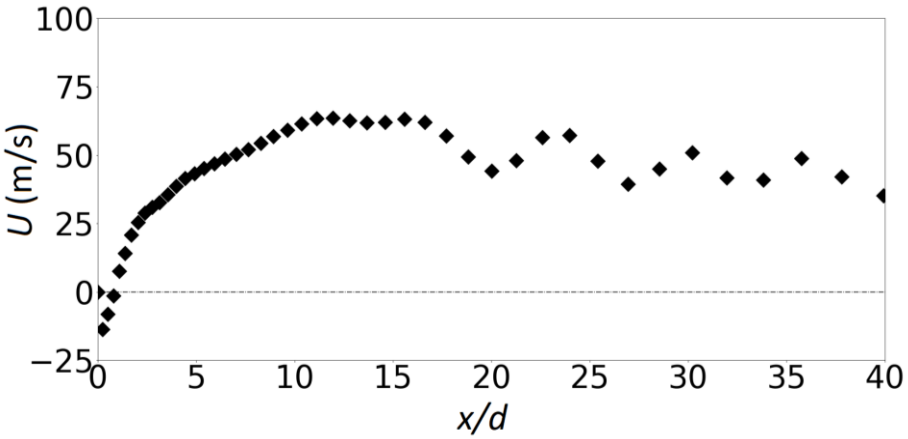

Fig. 15. Time-averaged streamwise velocity along the centerline for the two-orifice model

3.4 Instantaneous Velocity Magnitude

Figure 16 shows the instantaneous profiles of velocity magnitude at the A-A plane of the two-orifice model in Figure 1a at t/T = 0.4 and 0.5, for which the mean velocity and rms velocity fluctuations are shown in Figures 11d, 11e, 12d, and 12e, respectively. The phase-averaged velocity reaches its maximum value at around x/d = 15. However, in Figure 12d, rms fluctuations attain their maximum value at about x/d = 26. In Figure 16a, x/d = 26 roughly corresponds to the position of the end of the merging region, where the value of rms fluctuations significantly increases due to the jet interaction. This is also shown similarly when we compare Figures 12e and 16b: the maximum value of rms fluctuations is observed at about x/d = 32, which corresponds to the end of the merging region in the instantaneous velocity profile. We have also observed a similar tendency for the jet merging point and the rms velocity fluctuations for the four-orifice model.

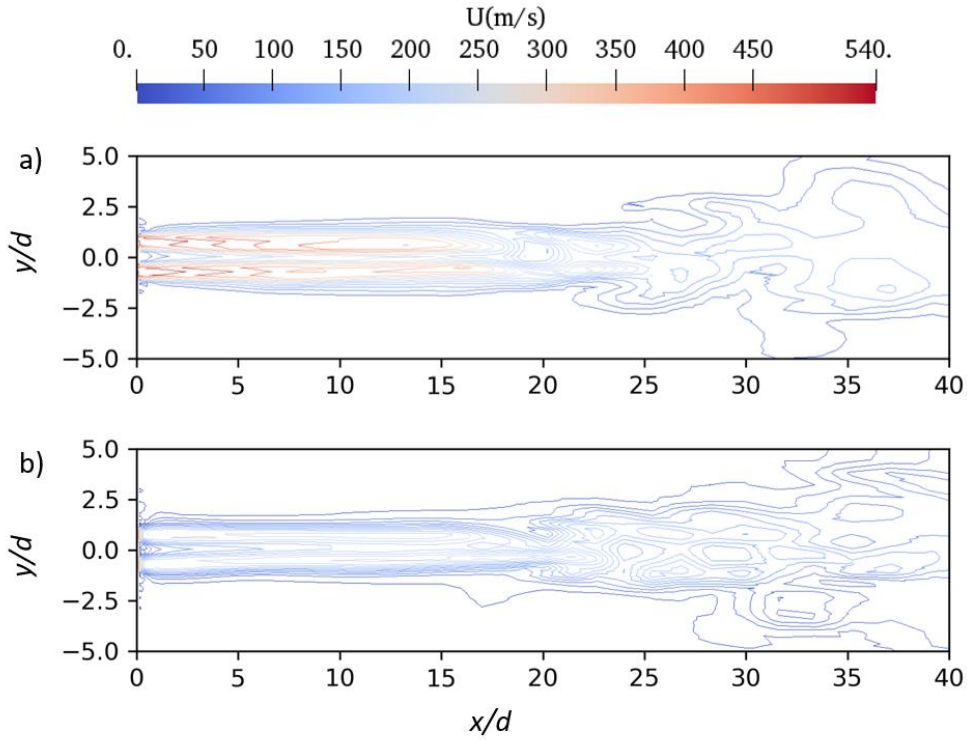

Fig. 16. Instantaneous distribution of the velocity magnitude on the A-A plane of the two-orifice model at a) *t/T* = 0.4 and b) *t/T* = 0.5

3.5 PDF of Velocity Fluctuations

The probability density function (PDF) of velocity fluctuations u' from the phase-averaged velocity is evaluated on the centerline of the flow at *x/d* = 5, 10, and 15. Hereafter, the PDF is normalized by the rms velocity fluctuations. Figure 17 plots the PDF for the two-orifice model at *t/T* = 0.4 and 0.8, which are in the blowing and suction phases, respectively. For comparison, a Gaussian distribution for PDF is shown with a broken red line in each figure. Although scatters are not negligible because of the limited number of samples, the distribution is still useful to discuss a general trend of the deviation from the Gaussian function. In the blowing phase of *t/T* = 0.4, a peak of the PDF appears for $u' > 0$, and the distribution deviates from the Gaussian function. Here, the PDF is negatively skewed, and a very large reversal velocity is observed at a low probability. A similar deviation of a PDF of velocity fluctuations was also reported for the interaction of continuous jets, even though a fully developed single jet has a Gaussian PDF along the jet centerline [12]. The PDF in the suction phase of *t/T* = 0.8 is closer to the Gaussian function than that in the blowing phase. Therefore, the suction due to the PSJA does not induce extremely large velocity fluctuations. Figure 18 shows the PDF for the four-orifice model along the centerline. Unlike the two-orifice model, the PDF is not negatively skewed for the four-orifice model, and the flow caused by the interaction of four synthetic jets does not accompany by very large negative velocity fluctuations.

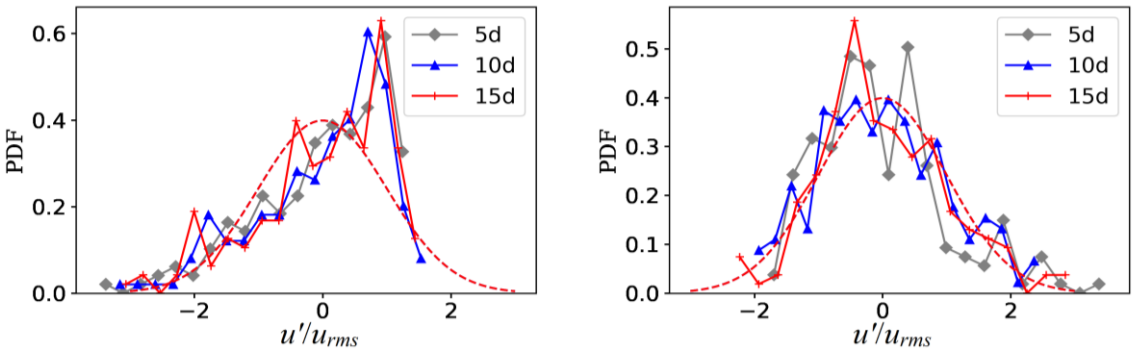

Fig. 17. PDF of u'/u_{rms} at x/d = 5, 10, and 15 along the centerline of the PSJA for the two-orifice model: a) t/T = 0.4 and b) t/T = 0.8. A red broken line represents a Gaussian distribution

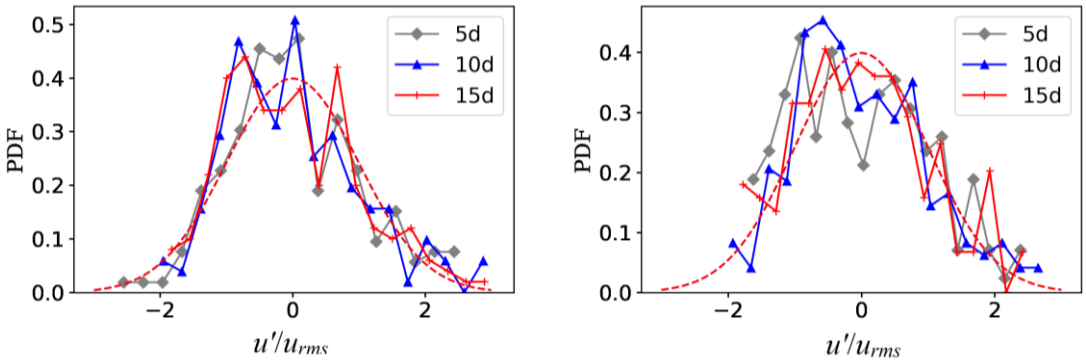

Fig. 18. Same as Figure 17 but for the four-orifice model

4. Conclusions

The flow properties of the piston synthetic jet actuator (PSJA) with two and four orifices are investigated with LES, which is carried out with OpenFOAM by modeling the piston movement with moving mesh. The flow generated by the PSJA with multiple orifices is examined for a wide range of actuation frequencies. Regardless of the number of orifices and the frequency, temporal variations of the pressure inside the actuator and the Mach number at the orifice exit are almost identical for different cycles, confirming that the jets are repeatedly generated under the same conditions. The maximum jet Mach number observed in the blowing phase is related to the maximum pressure inside the actuator, and their relationship for both two- and four-orifice models is well described by the theory for a flow inside a nozzle.

The interaction of synthetic jets generated by the two- and four-orifice models is investigated with the statistics conditioned on the phase. Slightly before the end of the blowing phase, the typical three regimes of the interaction reported for continuous jets [9] are observed for the synthetic jets: the converging region, where the jets are inclined toward the other jets; the merging region, where the synthetic jets interact; a combined region with a single jet formed from the multiple synthetic jets. Due to the time-dependent feature of the synthetic jets, the locations of these regions vary with time. Specifically, the jets tend to be parallel to each other at the beginning of the blowing phase, for which the converging region is not clearly observed. Therefore, the jets are not combined until a later stage of the blowing phase. These features are observed for both two- and four-orifice models. At the beginning of the blowing phase, the rms velocity fluctuations are large near the furthest locations where the jets reach. However, once the interaction of the synthetic jets occurs, large rms velocity fluctuations are observed at the downstream end of the merging region. As the merging region is shifted toward the downstream region with time in the blowing phase, the location where the rms

velocity fluctuations attain the maximum also varies with time. We have also examined the PDF of velocity fluctuations. For a fixed frequency, the flow generated by the two-orifice model has stronger intermittency in the blowing phase than that for the four-orifice model. This intermittent behavior results in a skewed distribution of the PDF. However, the deviation of the PDF from a Gaussian function is not significant for the suction phase. The present results for the interaction of the synthetic jets generated by the PSJAs will be useful for future applications in developing devices for flow control and the facilities to generate compressible turbulence.

Acknowledgement
This work was also supported by JSPS KAKENHI Grant Numbers 22K03903 and 22H01398.

References

[1] Glezer, Ari, and Michael Amitay. "Synthetic jets." *Annual review of fluid mechanics* 34, no. 1 (2002): 503-529. https://doi.org/10.1146/annurev.fluid.34.090501.094913

[2] Smith, Barton L., and Ari Glezer. "The formation and evolution of synthetic jets." *Physics of fluids* 10, no. 9 (1998): 2281-2297. https://doi.org/10.1063/1.869828

[3] Smith, Barton L., and G. W. Swift. "A comparison between synthetic jets and continuous jets." *Experiments in fluids* 34 (2003): 467-472.

[4] Iuso, Gaetano, and Gaetano Maria Di Cicca. "Interaction of synthetic jets with a fully developed turbulent channel flow." *Journal of turbulence* 8 (2007): N11. https://doi.org/10.1080/14685240601110088

[5] Honohan, Andrew, Michael Amitay, and Ari Glezer. "Aerodynamic control using synthetic jets." In *Fluids 2000 Conference and Exhibit*, p. 2401. 2000. https://doi.org/10.2514/6.2000-2401

[6] Hwang, W., and J. K. Eaton. "Creating homogeneous and isotropic turbulence without a mean flow." *Experiments in Fluids* 36 (2004): 444-454. https://doi.org/10.1007/s00348-003-0742-6

[7] Variano, Evan A., Eberhard Bodenschatz, and Edwin A. Cowen. "A random synthetic jet array driven turbulence tank." *Experiments in fluids* 37 (2004): 613-615. https://doi.org/10.1007/s00348-004-0833-z

[8] Pudsey, Adrian S., Vincent Wheatley, and Russell R. Boyce. "Behavior of multiple-jet interactions in a hypersonic boundary layer." *Journal of Propulsion and Power* 31, no. 1 (2015): 144-155. https://doi.org/10.2514/1.B35298

[9] Nasr, A., and J. C. S. Lai. "Comparison of flow characteristics in the near field of two parallel plane jets and an offset plane jet." *Physics of fluids* 9, no. 10 (1997): 2919-2931. https://doi.org/10.1063/1.869404

[10] Ghahremanian, Shahriar, Klas Svensson, Mark J. Tummers, and Bahram Moshfegh. "Near-field mixing of jets issuing from an array of round nozzles." *International Journal of Heat and Fluid Flow* 47 (2014): 84-100.https://doi.org/10.1016/j.ijheatfluidflow.2014.01.007

[11] Laban, Andrew, Seyed Sobhan Aleyasin, Mark Francis Tachie, and Mike Koupriyanov. "Experimental investigation of nozzle spacing effects on characteristics of round twin free jets." *Journal of Fluids Engineering* 141, no. 7 (2019): 071201. https://doi.org/10.1115/1.4041989

[12] Zhou, Yi, Koji Nagata, Yasuhiko Sakai, and Tomoaki Watanabe. "Dual-plane turbulent jets and their non-Gaussian velocity fluctuations." *Physical Review Fluids* 3, no. 12 (2018): 124604. https://doi.org/10.1103/PhysRevFluids.3.124604

[13] Ali, Mohd Yousuf, and Farrukh Alvi. "Jet arrays in supersonic crossflow—An experimental study." *Physics of fluids* 27, no. 12 (2015).https://doi.org/10.1063/1.4937349

[14] Yaacob, Mohd Rusdy, Rasmus Korslund Schlander, Preben Buchhave, and Clara M. Velte. "Experimental evaluation of kolmogorov's-5/3 and 2/3 power laws in the developing turbulent round jet." *Journal of Advanced Research in Fluid Mechanics and Thermal Sciences* 45, no. 1 (2018): 14-21.

[15] Bisoi, Mukul, Manab Kumar Das, Subhransu Roy, and Devendra Kumar Patel. "Turbulent statistics in flow field due to interaction of two plane parallel jets." *Physics of Fluids* 29, no. 12 (2017). https://doi.org/10.1063/1.5018306

[16] Zhou, Yi, Koji Nagata, Yasuhiko Sakai, Tomoaki Watanabe, Yasumasa Ito, and Toshiyuki Hayase. "Energy transfer in turbulent flows behind two side-by-side square cylinders." *Journal of Fluid Mechanics* 903 (2020): A4. https://doi.org/10.1017/jfm.2020.611

[17] Zhou, Yi, Koji Nagata, Yasuhiko Sakai, and Tomoaki Watanabe. "Extreme events and non-Kolmogorov spectra in turbulent flows behind two side-by-side square cylinders." *Journal of Fluid Mechanics* 874 (2019): 677-698.https://doi.org/10.1017/jfm.2019.456

[18] Smith, Barton, Mark Trautman, and Ari Glezer. "Controlled interactions of adjacent synthetic jets." In *37th aerospace sciences meeting and exhibit*, p. 669. 1999.https://doi.org/10.2514/6.1999-669

[19] Guo, Dahai, Linda Kral, and Andrew Cary. "Numerical simulation of the interaction of adjacent synthetic jet actuators." In *Fluids 2000 Conference and Exhibit*, p. 2565. 2000. https://doi.org/10.2514/6.2000-2565

[20] Jabbal, Mark, Stephen Liddle, Jonathan Potts, and William Crowther. "Development of design methodology for a synthetic jet actuator array for flow separation control applications." *Proceedings of the Institution of Mechanical Engineers, Part G: Journal of Aerospace Engineering* 227, no. 1 (2013): 110-124. https://doi.org/10.1177/0954410011428256

[21] Jankee, Girish K., and Bharathram Ganapathisubramani. "Interaction and vectoring of parallel rectangular twin jets in a turbulent boundary layer." *Physical Review Fluids* 6, no. 4 (2021): 044701.https://doi.org/10.1103/PhysRevFluids.6.044701

[22] Ariffin, Ahmad Hamdan, and Kamarul Ariffin Ahmad. "Computational Fluid Dynamic (CFD) Simulation of Synthetic Jet Cooling: A Review." *Journal of Advanced Research in Fluid Mechanics and Thermal Sciences* 72, no. 2 (2020): 103-112. https://doi.org/10.37934/arfmts.72.2.103112

[23] Husin, Azmi, Mohd Zulkifly Abdullah, Azmi Ismail, Ayub Ahmed Janvekar, Mohd Syakirin Rusdi, and Wan Mohd Amri Wan Mamat Ali. "Heat Transfer Performance of a Synthetic Jet Generated by Diffuser-Shaped Orifice." *Journal of Advanced Research in Fluid Mechanics and Thermal Sciences* 53, no. 1 (2019): 122-128.

[24] Zhang, Min, Taiho Yeom, Youmin Yu, Longzhong Huang, Terrence W. Simon, Mark T. North, and Tianhong Cui. "Development of Synthetic Jet Arrays for Heat Transfer Enhancement in Air-Cooled Heat Sinks for Electronics Cooling." In *Heat Transfer Summer Conference*, vol. 44786, pp. 601-606. American Society of Mechanical Engineers, 2012. https://doi.org/10.1115/HT2012-58092

[25] Crittenden, Thomas M., and Ari Glezer. "A high-speed, compressible synthetic jet." *Physics of Fluids* 18, no. 1 (2006). https://doi.org/10.1063/1.2166451

[26] Gilarranz, J. L., L. W. Traub, and O. K. Rediniotis. "A new class of synthetic jet actuators—Part I: Design, fabrication and bench top characterization." *J. Fluids Eng.* 127, no. 2 (2005): 367-376. https://doi.org/10.1115/1.1839931

[27] Gilarranz, J.L., Traub, L.W., Rediniotis, O.K., "A New Class of Synthetic Jet Actuators—Part II: Application to Flow Separation Control," *Journal of Fluids Engineering,* Vol.127, pp. 377-387, (2005). https://doi.org/10.1115/1.1882393

[28] Sakakibara, Hiroyuki, Tomoaki Watanabe, and Koji Nagata. "Supersonic piston synthetic jets with single/multiple orifice." *Experiments in Fluids* 59 (2018): 1-12. https://doi.org/10.1007/s00348-018-2529-9

[29] Tung, Pham Duy, Tomoaki Watanabe, and Koji Nagata. "Large-Eddy Simulation of a Flow Generated by a Piston-driven Synthetic Jet Actuator." *CFD Letters* 15, no. 8 (2023): 1-18. https://doi.org/10.37934/cfdl.15.8.118

[30] Yamamoto, Kohei, Tomoaki Watanabe, and Koji Nagata. "Turbulence generated by an array of opposed piston-driven synthetic jet actuators." *Experiments in Fluids* 63, no. 1 (2022): 35. https://doi.org/10.1007/s00348-021-03351-z

[31] Yamamoto, K., T. Ishida, T. Watanabe, and K. Nagata. "Experimental and numerical investigation of compressibility effects on velocity derivative flatness in turbulence." *Physics of Fluids* 34, no. 5 (2022). https://doi.org/10.1063/5.0085423

[32] Zhao, Majie, Yifan Bian, Qinling Li, and Taohong Ye. "Large eddy simulation of transverse single/double jet in supersonic crossflow." *Aerospace Science and Technology* 89 (2019): 31-45. https://doi.org/10.1016/j.ast.2019.03.044

[33] Eri, Qitai, Liang Hong, and Ting Li. "Novel Piston-Type Synthetic Jet Actuator with Auxiliary Air Inlet." *Journal of Aerospace Engineering* 32, no. 1 (2019): 04018127. https://doi.org/10.1061/(ASCE)AS.1943-5525.0000936

[34] J. Anderson, Modern Compressible Flow: With Historical Perspective, McGraw-Hill, (1990).

[35] Kim, Museong, Hoonsang Lee, and Wontae Hwang. "Experimental study on the flow interaction between two synthetic jets emanating from a dual round orifice." *Experimental Thermal and Fluid Science* 126 (2021): 110400. https://doi.org/10.1016/j.expthermflusci.2021.110400